https://doi.org/10.5194/egusphere-2026-1733
Preprint. Discussion started: 8 May 2026

Hot extremes following net-zero CO_2 emissions in UKESM: physical drivers and role of vegetation

Andrea Rivosecchi [1,2], Andrea Dittus [1,3], Ed Hawkins [1,3], Reinhard Schiemann [1,3], and Erich Fischer [4]

[1]Department of Meteorology, University of Reading, Reading, United Kingdom

[2]Impacts on Agriculture, Forestry and Ecosystem Services (IAFES) Division, Euro-Mediterranean Center on Climate Changes (CMCC), Sassari, Italy

[3]National Centre for Atmospheric Science, Reading, United Kingdom

[4]Institute for Atmospheric and Climate Science, ETH Zurich, Zurich, Switzerland

Correspondence: Andrea Rivosecchi (a.rivosecchi@pgr.reading.ac.uk)

https://doi.org/10.5194/egusphere-2026-1733
Preprint. Discussion started: 8 May 2026

Abstract. Reaching net-zero CO_2 emissions is essential to halt continuing global warming and attempt to stabilise global temperatures. However, large uncertainties remain on the sign and the magnitude of the long-term responses of the climate system following anthropogenic emissions cessation. This study contributes to improving our understanding of the climate system post CO_2 emissions cessation, by exploring the global and regional temperature evolution in UKESM1.2 following the TIPMIP protocol. Zero CO_2 emission simulations, starting from global warming levels of +1.5°C to +5°C above pre-industrial are analysed to understand the impact of historical cumulative emissions and associated global warming level on post zero-emissions trends. We find that the global average surface air temperature (GSAT) keeps increasing in all zero CO_2 emission UKESM1.2 projections. The increase is more pronounced at higher warming levels, approaching 0.25°C per century in the +3.0°C to +5.0°C scenarios. Most of the warming occurs in the Southern Hemisphere, particularly in the Southern Ocean, while the Northern Hemisphere land experiences a slight cooling trend. These regional cooling trends are more marked for the annual temperature maxima, with several regions across 45-65°N experiencing cooling of >1°C per century. We find the strongest regional cooling trend following emissions cessation in the higher warming scenarios. Here, we investigate the drivers behind the cooling trend in northeastern North America, where the cooling magnitude exceeds 1.5°C per century. We find that the cooling trend is almost completely explained by thermodynamic drivers. We reconcile this finding with the UKESM1.2 dynamic vegetation changes, as the evergreen vegetation cover increases across all regions experiencing substantial cooling in the hot extremes. This finding highlights the significant regional contribution that vegetation changes can have for the attenuation of annual temperature maxima, supporting the case for their careful consideration in future mitigation and adaptation strategies. However, these results also show the limitations of highly idealised scenario protocols like TIPMIP, which set crop and pasture distributions, as well as other anthropogenic forcings, to pre-industrial values, allowing vegetation to expand freely. This highlights the importance of developing new zero emissions protocols considering other forcing agents beyond CO_2.

1 Introduction

With 2024 marking the first year with global average surface air temperature (GSAT) rising 1.5°C above pre-industrial conditions, mitigation efforts need to rapidly accelerate in order to limit global warming to the Paris Agreement targets (WMO, 2025). Reaching global net-zero CO_2 emissions is fundamental to achieve long-term stabilisation of global average temperatures and limit the negative impacts of global warming (Hoegh-Guldberg et al., 2018). Thus, increasing attention has been given to understanding the implications of a stabilising state of the climate system, as most of our current knowledge is based on the study of transient conditions. Researching the post net-zero changes to the climate system serves the double purpose of further informing policymakers of the benefits deriving from CO_2 emission cessation while preparing them to the global and regional adaptation challenges we will still have to face (Winkelmann et al., 2025; Jones et al., 2019).

The stabilising effect of CO_2 emission cessation on global average temperatures is long established, and mainly results from the balance of declining atmospheric concentration due to natural carbon sinks and the reduced ocean heat uptake efficiency (Lee et al., 2021). Yet, significant uncertainties remain on the sign and the magnitude of the long-term GSAT trend, as different

https://doi.org/10.5194/egusphere-2026-1733
Preprint. Discussion started: 8 May 2026

components of the climate system will adjust on different timescales to the forcing cessation (Corner et al., 2023; MacDougall et al., 2020). At the regional level, this uncertainty translates to sharp geographical differences in precipitation and temperature trends following climate stabilisation (King et al., 2024a; Dittus et al., 2024). At the same time, a GSAT uncertainty of even a fraction of a degree has an amplified effect on climate extremes, with discernible differences in their intensity and frequency emerging at every 0.1°C increment (Lee et al., 2021). The present study aims to help constrain these sources of uncertainty by providing further evidence on the response of mean and extreme temperature indicators following CO_2 emissions cessation at different stabilised warming levels (swl). In this perspective, the analysis complements and expands the results of the few other works that have so far investigated changes in temperature extremes following zero emission conditions (Cassidy et al., 2024; Alastrué de Asenjo et al., 2025; Perkins-Kirkpatrick et al., 2025). After an initial exploratory analysis of the mean global temperature response to emissions cessation, we investigate changes in the annual temperature hot extremes and attempt to identify the physical drivers behind their regional changes.

2 Methods

2.1 Model protocol and projections

The analysis is based on the climate projections produced by the UK Earth System Model version 1.2 (UKESM1.2) following the Tipping Points Model Intercomparison Project (TIPMIP) protocol (Winkelmann et al., 2025; Jones et al., 2025). UKESM1.2 is equivalent to UKESM1.1 (Mulcahy et al., 2023), with the addition of interactive Greenland and Antarctic ice sheets (Smith et al., 2021; Siahaan et al., 2022). Three sets of climate projections are developed as part of TIPMIP and were used in this study: 1) transient climate projections, referred to as "ramp-up" in the text, where CO_2 emissions are kept at a fixed rate of 80 Gt CO_2 per century to produce an historical-like warming rate of 2°C per century; 2) zero emissions projections, where CO_2 emissions are set to 0 and the atmospheric concentration changes based on natural feedback mechanisms; 3) net-negative projections, where CO_2 atmospheric concentration decreases at a rate of 40 Gt CO_2 per century simulating active anthropogenic removal. The zero emissions runs branch off directly from the transient run once the specified global warming levels are achieved. The global warming levels are defined as the GSAT anomaly above the value at the beginning of the ramp-up. This is calculated by comparing a 31-year average of GSAT at any point in the ramp-up run to the equivalent centred around the branching point of the ramp-up run from the pi-Control run. Similarly, net-negative runs branch off directly from the zero emissions runs after a stabilisation period following the emissions cessation date. All the simulations are run with CO_2-only forcing, with other gases and aerosols fixed at the pre-industrial level (Winkelmann et al., 2025). The projections have a dynamic land surface and vegetation module based on the Joint UK Land Environment Simulator (JULES) (Clark et al., 2011; Harper et al., 2016, 2018), with cropland and pasture kept constant at the pre-industrial level (Jones et al., 2025). Here we analyse the stabilised warming level runs branching from the ramp-up at 1.5, 2, 3, 4 and 5°C, as these offered the greatest data availability at the time of the analysis. Three ensemble members were available for the transient and zero emissions projections and one for the net-negative runs. In each set of runs, the analysis is conducted considering a period of 250 years from the starting date.

https://doi.org/10.5194/egusphere-2026-1733
Preprint. Discussion started: 8 May 2026

2.2 Annual temperature extremes: TXx and TX5x

Annual temperature extremes are calculated from the daily maximum temperature data. TXx is defined as the daily maximum temperature during the hottest day of the year, while TX5x represents the hottest 5-day period calculated as the annual highest 5-day average daily maximum temperature. The trends in these metrics are calculated using a linear polynomial fit.

2.3 Surface heat fluxes

Daily data on sensible and latent heat fluxes are used to evaluate changes in turbulent fluxes between the Earth's surface and the lower troposphere associated with changes in surface temperature. An extensive body of literature has shown how the partitioning of surface heat fluxes regulates the intensity of hot temperature extremes (Seneviratne et al., 2010; Miralles et al., 2019), exacerbating them when exceptionally dry conditions occur (Fischer et al., 2007; Perkins et al., 2015). Here, we use the evaporative fraction (EF) to monitor how the latent heat component is changing compared to the total surface flux (Donat et al., 2017), as shown in equation 1:

$$EF = \frac{LH}{LH + SH} \tag{1}$$

where LH and SH are the latent and sensible heat fluxes (W m^{-2}), respectively. This metric has found wide application in the literature as an indicator of the partitioning of available energy, with higher values indicating wetter conditions and vice-versa (Ukkola et al., 2018; Costa et al., 2022).

2.4 Atmospheric circulation analogues

To further analyse the changes in the drivers of annual temperature extremes and understand which factors primarily contribute to their regional evolution under zero CO_2 emissions conditions, we use an approach based on circulation analogues similar to Deser and Phillips (2016) and Horowitz et al. (2022). This method aims to understand the extent that atmospheric circulation conditions leading to extreme temperatures at the beginning of the stabilised period could reproduce the same effects later in the run. Here, a set of 20 randomly sampled TX5x events (see below) occurring in the years 50-150 (early) and 150-250 (late) of the zero emissions projections is selected as target events. For the construction of the circulation analogues, the temperature, sea level pressure (slp) and 500 hPa geopotential height (zg500) data are linearly detrended and their seasonal cycle removed prior to the analysis (Deser and Phillips, 2016). TX5x events are calculated from the spatially averaged daily maximum temperature field over the selected region to avoid the risk of selecting different events across the studied region. The five dates of each event are then used to extract the corresponding daily slp and zg500 fields. For each of those slp and zg500 target patterns, circulation analogues are identified in the UKESM1.2 piControl run. Each analogue is drawn from a different year, with the selected pattern having the smallest Euclidean distance to the target slp fields. The analysis was also repeated drawing analogues from the zg500 fields, as both approaches were used in previous studies (Merrifield et al., 2017; Horowitz

https://doi.org/10.5194/egusphere-2026-1733
Preprint. Discussion started: 8 May 2026

et al., 2022). The Euclidean distance is calculated for a subsection of the slp fields spanning 54° west, 18° east, 15° north, and 15° south of the centre of the studied region in order to capture typical wave patterns associated with heat extremes in North America (Horowitz et al., 2022). To allow for seasonal consistency in the pressure-temperature relationship, the analogues were only selected from a time window of 14 days centred around the initial day of the target TX5x event. To increase the robustness of the results, we draw analogues for a randomly selected subsample of 20 of the 100 target events in each half of the stabilised warming projection and repeat this procedure 30 times. As shown by Deser and Phillips (2016) and Horowitz et al. (2022), this number of iterations (30) combined with the total length of the period from which analogues are drawn (500 years), is sufficient to make the root mean square error of temperature and pressure analogues converge. Each of the analogue slp patterns (P_a) is then linearly regressed on the corresponding target slp patterns (P_t) to get a dynamical regression coefficient (β) linking the target slp fields to each of their analogues as in equation 2:

$$P_t = P_a\beta + e \tag{2}$$

where e is the residual.

Thus, β is used to estimate the dynamically induced component (T_{dc}) of the target temperature anomaly from the analogues temperature fields (T_a; equation 3):

$$T_{dc} = T_a\beta \tag{3}$$

Only the analogues with a resulting T_{dc} above the 85^{th} percentile of all identified analogues were considered. As explained in Horowitz et al. (2022), this avoids selecting pressure anomalies that do not produce significant temperature anomalies in the piControl. Finally, T_{dc} is averaged to get a mean dynamically induced temperature value for the target TX5x events in the early (years 50-150) and late (years 150-250) parts of the stabilised emission run. Thus, the difference between the target events temperature and the dynamically induced component represents the residual contribution to temperature due to thermodynamic drivers.

3 Results

3.1 Mean Temperature trends

The GSAT shows a warming trend (0.01°C - 0.24°C century^{-1}) in the ensemble mean after reaching net-zero emissions in all swl scenarios analysed (Figure 1). The same applies to all individual ensemble members except for swl-2.0, where a slight cooling trend is projected in two ensemble members. The warming trend is stronger in swl-3.0, swl-4.0 and swl-5.0 (0.23 - 0.24 °C century^{-1}) compared to the lower warming levels (0.01 - 0.05 °C century^{-1}). This warming-level dependency

https://doi.org/10.5194/egusphere-2026-1733
Preprint. Discussion started: 8 May 2026

of the post-zero emission global temperature trends seen in UKESM1.2, also known as the Zero Emission Commitment, is documented and analysed in detail in a preprint by Gibbs et al. (2026). Continued warming after emissions cessation was also reported by King et al. (2024a) analysing similar stabilised warming projections from ACCESS-ESM-1.5. However, they found a significantly weaker warming trend (0.03-0.05°C per century) and did not report the same warming-level dependency on the trend magnitude. A multi-model assessment of the Zero-Emission Commitment Model Intercomparison Project (ZECMIP) by MacDougall et al. (2020) pointed out how a previous version of UKESM (UKESM1.0-LL) showed an even higher warming trend post zero emissions to what is observed here (+0.75°C after 90 years following 2000 PgC cumulative CO_2 emissions). The same study highlighted how there is significant model-dependent uncertainty in the GSAT evolution after emissions stop, with models also showing diverging responses depending on the amount of antecedent cumulative CO_2 emissions. Indeed, this uncertainty derives from the multitude of climate system feedbacks, involving the ocean, the biosphere and the atmosphere, contributing to the planetary re-equilibration post emission cessation (Corner et al., 2023).

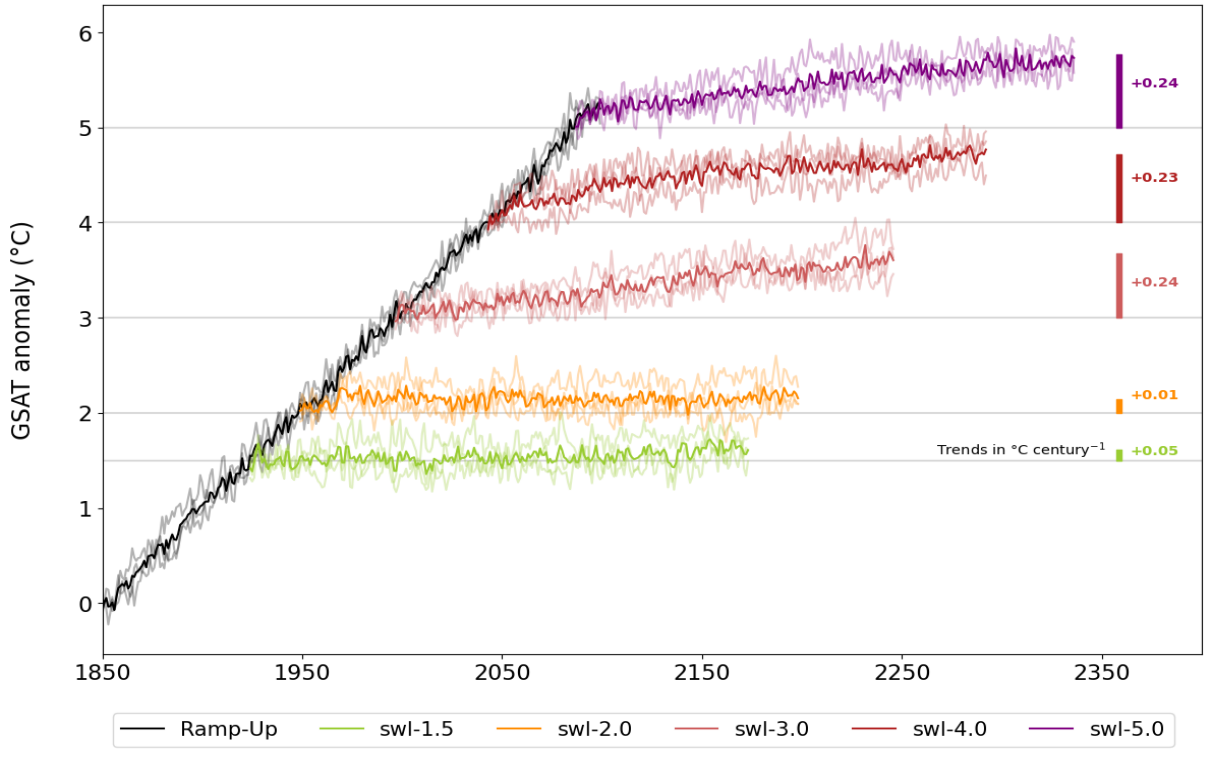

Figure 1. *Time series of the global average surface air temperature anomaly (GSAT) in the ramp-up and swl-1.5, 2.0, 3.0, 4.0 and 5.0 runs in UKESM1.2 under the TIPMIP protocol. The solid line shows the ensemble mean, with the faded lines representing the individual ensemble members. The coloured bars visually represent the GSAT anomaly change throughout the entire run, with the centennial trend labelled next to them.*

Analysing the temperature trends spatially, we find that the mean temperature evolution after emissions stop is not globally homogeneous, but sharp regional contrasts apply (Figure 2). Consistent with previous modelling studies (King et al., 2024a;

https://doi.org/10.5194/egusphere-2026-1733
Preprint. Discussion started: 8 May 2026

Gillett et al., 2011; Frölicher et al., 2014), the strongest warming trend in UKESM1.2 is found in the Southern Ocean (SO) at all stabilised warming levels. Again, a sharp contrast appears between the two coldest runs (swl-1.5 and swl-2.0) and the others. In the former, the warming pattern is almost exclusively confined to the SO and slight cooling occurs over global land masses. In contrast, warmer runs show amplified warming in the SO and widespread temperature increases over land masses, especially in the Southern Hemisphere (SH). Notably, a cooling trend of approximately 0.5°C century^{-1} is observed at the regional scale across the Northern Hemisphere (NH) in the swl-4.0 and swl-5.0 runs, particularly over northeastern North America, southern Siberia and northeastern China.

https://doi.org/10.5194/egusphere-2026-1733
Preprint. Discussion started: 8 May 2026

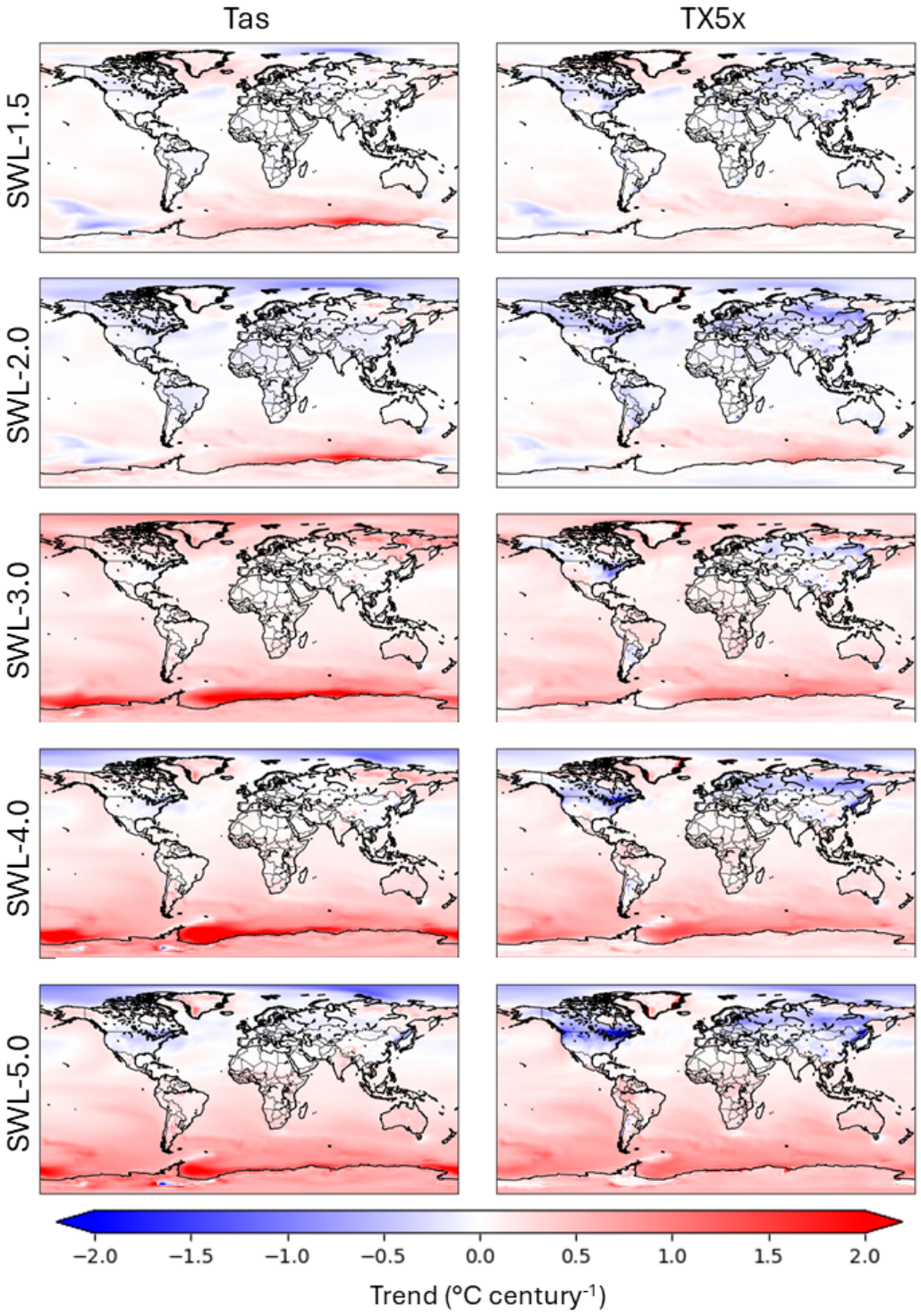

Figure 2. *Left: average annual surface air temperature (Tas) trend (°C century^{-1}) in the ensemble mean of all stabilised warming level runs analysed (swl-1.5 to swl-5.0). Trends are calculated considering the first 250 years after* CO_2 *emissions cessation in each swl run. Right: same as left, but for TX5x.*

https://doi.org/10.5194/egusphere-2026-1733
Preprint. Discussion started: 8 May 2026

3.2 Extreme temperature trends

The global pattern of the annual hot extremes resembles the features shown in the mean temperature analysis, but some substantial differences can be identified at the regional scale (Figure 2). First, in swl-1.5 and swl-2.0 TX5x shows a more widespread cooling trend over land compared to Tas, encompassing most of NH and stretching into South America. TX5x also exhibits a stronger cooling trend over land in the warmer runs, where it has an approximately zonal pattern at 45-65°N (Figure 2). Similar to the mean temperature, the largest cooling for TX5x also occurs regionally in North America, southern Siberia and northeastern China in swl-4.0 and 5.0. Yet, the cooling magnitude in these regions is greater for the warm tail of the annual temperature distribution (-1 to -1.5°C century^{-1}) than for the mean (Figure 2). In contrast to the trend in the mean, cooling of TX5x also appears locally in the SH, particularly in New Zealand and southern Chile (Figure 2). While not as pronounced as in the NH, cooling at these locations is particularly striking as it deviates from the widespread warming occurring elsewhere across the SH, and particularly the SO. Very similar trends are projected for TXx, matching almost perfectly TX5x (Figure 2) both spatially and in terms of magnitude (not shown).

Figure 3 provides a more detailed regional analysis of the evolution of the spatially averaged TX5x across the regions exhibiting a stronger cooling trend. The examined regions are northeastern North America [44 - 49°N; 75 – 64 °W], northeastern Asia [43 - 52°N ; 130 - 134°E], southern Chile [38 - 40°S ; 72°W] and southern New Zealand [44 - 45°S ; 168 - 170°E]. In all regions, all ensemble members agree on the strongest TX5x reduction occurring in the swl-4.0 and 5.0 scenarios. North America experiences the greatest cooling, with TX5x decreasing by more than 3°C throughout swl-5.0 and reaching lower values than at the beginning of the swl-3.0 run (Figure 3). Both NH regions experience cooling in the swl-1.5 and swl-2.0 scenarios, in line with the observed cooling of mean temperature (Figure 2), albeit smaller than what seen in the two warmest runs. Chile also experiences some cooling in swl-2.0, but this is three times smaller than in swl-4.0 and swl-5.0. The same regional analysis conducted for TXx produced very similar results (not shown).

https://doi.org/10.5194/egusphere-2026-1733
Preprint. Discussion started: 8 May 2026

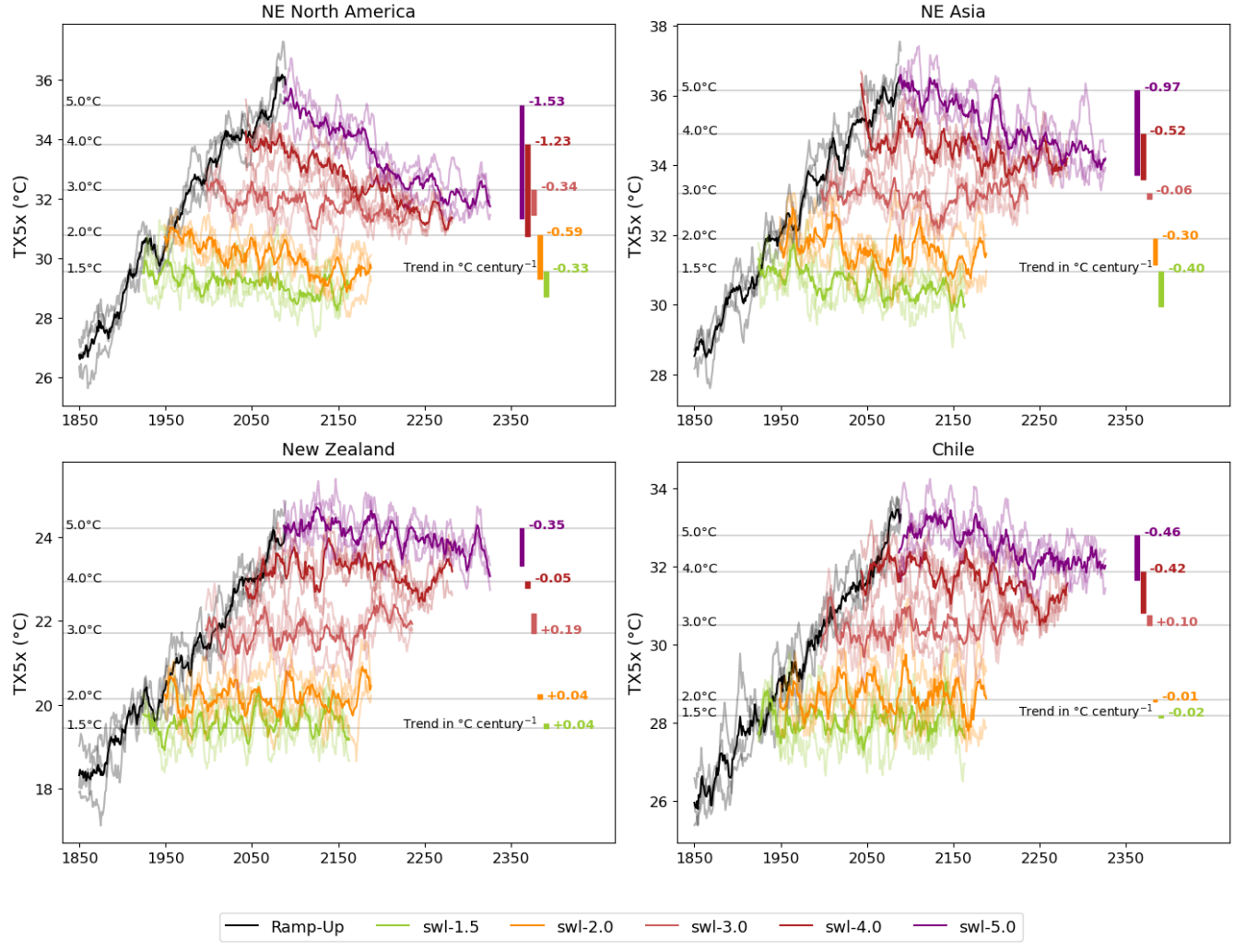

Figure 3. *Time series TX5x averaged over the studied regions of northeastern North America, northeastern Asia, New Zealand and Chile for the ramp-up and all the stabilised warming level projections. The time series are smoother with an 11-year filter to improve readability. The labelled bars on the right-hand side indicate the centennial TX5x trend in the ensemble mean of each swl, wit the grey horizontal lines representing the average value for the first 30 years.*

3.3 Drivers of hot extremes decline

Given the intensity and the spatial extent of the cooling trend affecting it, northeastern North America is used as a case study to investigate the causes behind the reduction in annual temperature extremes. The analysis is only conducted for TX5x since, as previously discussed, it shows almost identical trends and patterns to TXx (Figures 2,3). Moreover, TX5x represents a more robust metric than TXx to understand changes in hot temperature extremes of societal relevance, as its length approximates better the characteristic duration of heatwave events (Russo et al., 2019).

https://doi.org/10.5194/egusphere-2026-1733
Preprint. Discussion started: 8 May 2026

Changes in heatwave intensity result from a combination of dynamic and thermodynamic factors (Quesada et al., 2012; Perkins et al., 2015), with their relative importance varying regionally (Donat et al., 2017). While the former control the potential onset and duration of a heatwave event, the latter substantially affect the magnitude of warming (Seneviratne et al., 2010; Barriopedro et al., 2023). To identify the contribution from these components we use an approach based on atmospheric circulation analogues as explained in the Methods section (Deser and Phillips, 2016). Figure 4 shows the average daily maximum temperature anomaly associated with randomly sampled TX5x events (top row) in the early (years 50-150) and late (years 151-250) periods of swl-5.0 and their respective breakdown into the dynamical (middle row) and residual components (bottom row). The last column shows the difference in temperature anomaly between the two periods for the total and the individual components of the temperature anomaly. As shown before, TX5x events show a total cooling of approximately 1.5°C per century over the studied region (green box). Most of this cooling is associated with a weaker thermodynamical (i.e., residual) contribution, accounting for almost the entirety of the total difference over the studied region. Conversely, the dynamically induced contribution to the temperature anomaly is almost identical in the TX5x events in the two halves of swl-5.0 (Figure 4). As explained in the Methods, the analysis was repeated drawing circulation analogues based on the slp and zg500 fields yielding almost identical results (not shown).

https://doi.org/10.5194/egusphere-2026-1733
Preprint. Discussion started: 8 May 2026

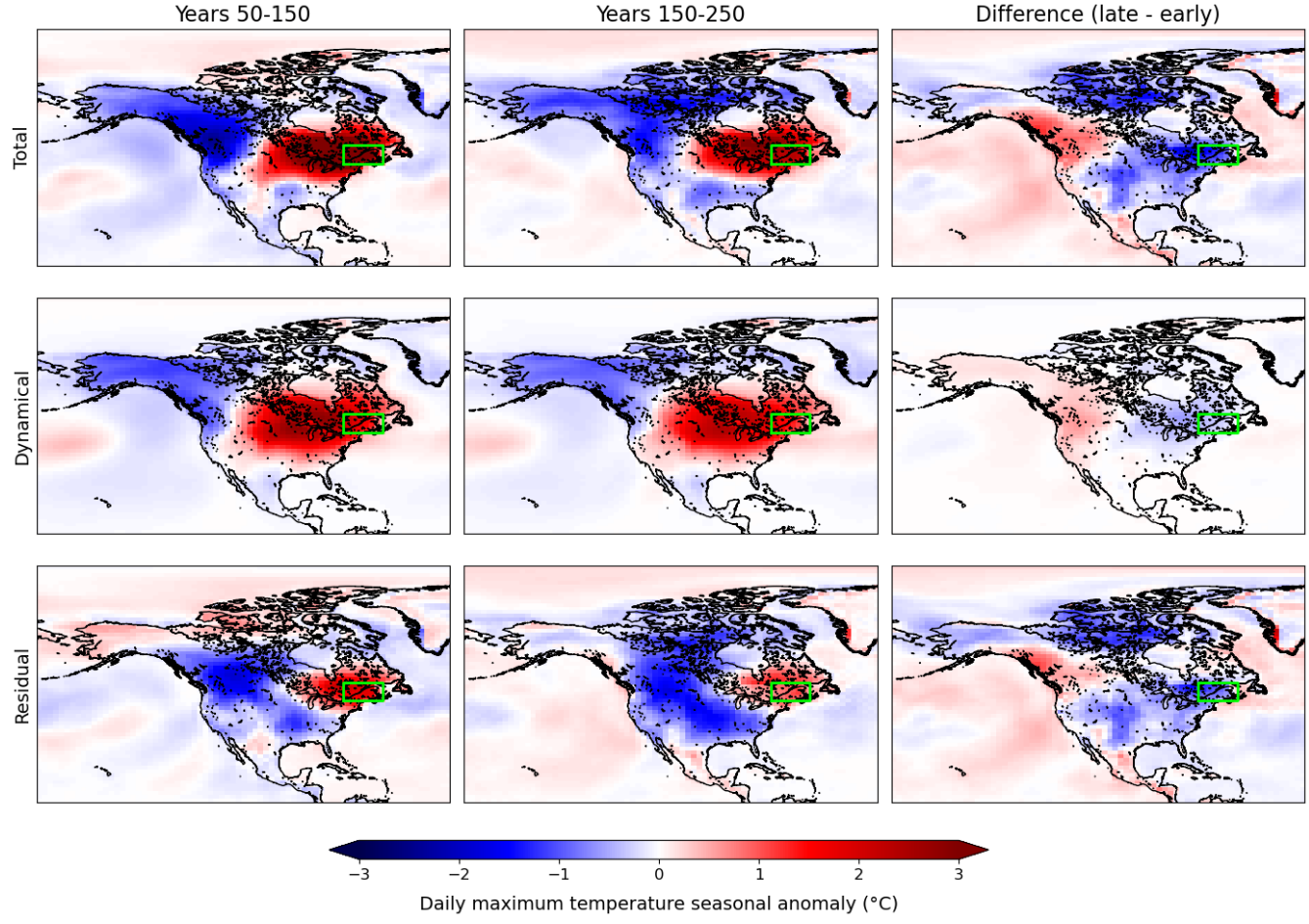

Figure 4. *Analysis of the drivers of TX5x events identified in the studied North American region (green box) in the early (years 50-150) and late (years 150-250) halves of swl-5.0 using circulation analogues drawn from UKESM1.2 piControl run (see Methods). The top row shows the average daily maximum temperature seasonal anomaly pattern for the selected target events in swl-5.0 and their difference. The middle row shows the dynamical component of the temperature forcing. The bottom row shows the difference between the former two as the residual. The last column shows the average difference between events sampled in the late and early parts of the run for each of the temperature anomaly components.*

Thus, we analysed the surface heat fluxes to seek further evidence of the contribution from land-atmosphere interactions to the cooling trend. In particular, we focused on the simultaneous evolution of TX5x and EF (see Methods) to understand whether the projected changes in temperature are accompanied by changes in latent and sensible heat fluxes. Figure 5 shows the relationship between TX5x and EF in the swl-2.0, swl-4.0 and swl-5.0, as well as the ramp-up run, combining data from all ensemble members. The figure shows how the decreasing trend in TX5x (highlighted by the solid lines) is associated with a concomitant increase in EF (0.04 per century) in swl-4.0 and swl-5.0. This suggests that, in these projections, a higher fraction of radiative forcing is dispersed upward through evaporation rather than directly warming the surface. This finding is consistent with the observed cooling trend and helps explain the non-dynamical component of this signal over North America.

https://doi.org/10.5194/egusphere-2026-1733
Preprint. Discussion started: 8 May 2026

This relationship, albeit reversed, also holds for the ramp-up run, where the rapid increase in TX5x goes together with a considerable reduction in EF. Notably, a much weaker association between TX5x and EF is found in the swl-2.0 projection, suggesting that surface heat fluxes might have a smaller influence on annual temperature extremes in this scenario.

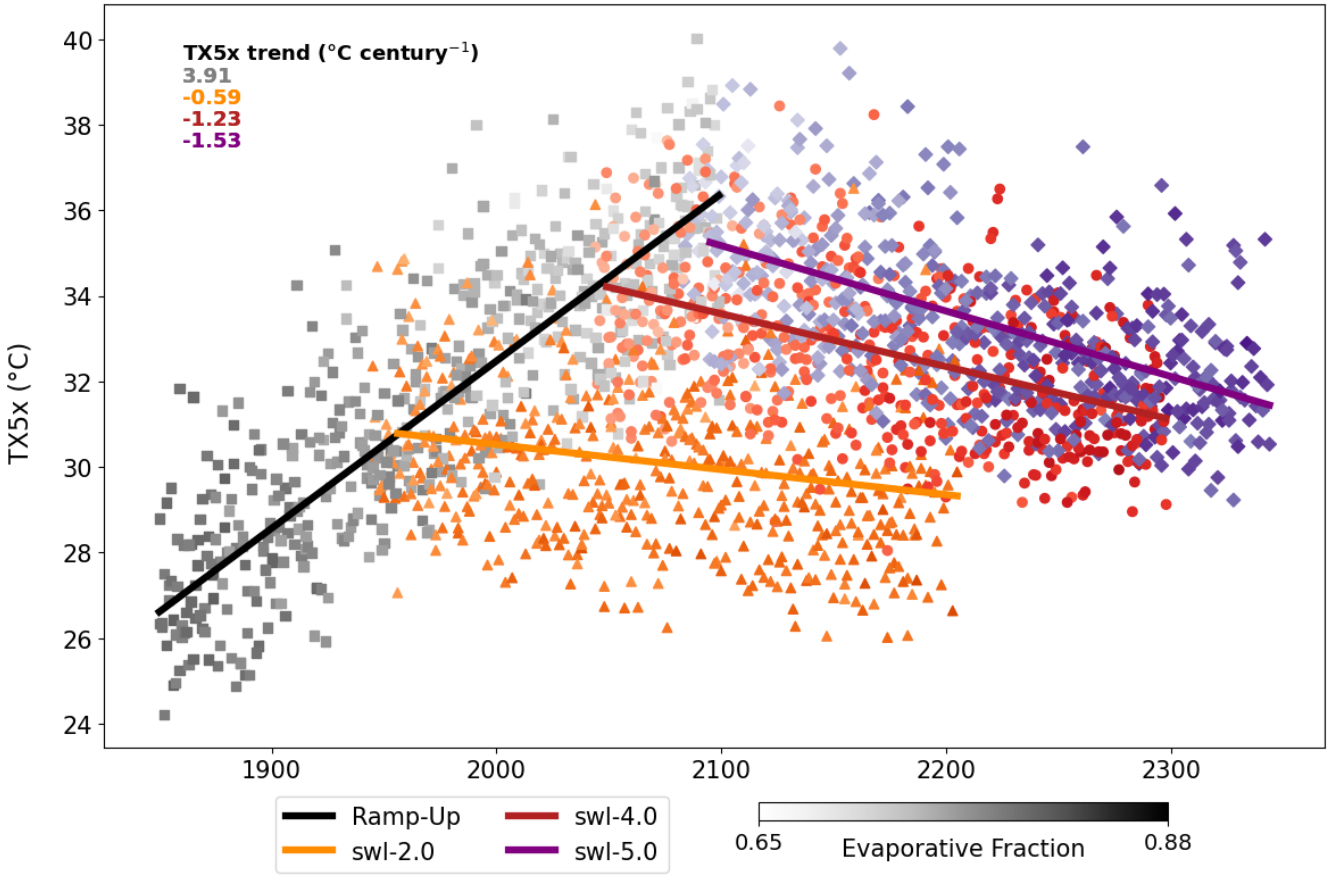

Figure 5. *Timeseries of annual TX5x values and mean summer (JJA) evaporative fraction (EF) values in all the ensemble members combined for the ramp-up (RUP, black squares), swl-2.0 (green triangles), 4.0 (red circles) and 5.0 (purple diamonds) scenarios. The colours shading indicates changes in EF, with higher values denoted by a darker shade. The solid lines indicate the mean TX5x linear trend across all ensemble members of a given scenario, with the corresponding numeric value noted on the top-left corner.*

3.4 The role of vegetation

The increase in the average summer latent heat fraction shown by the EF trend (Figure 5) suggests an upward trend of water availability in the region. The model output for precipitation and surface soil moisture do not show a direct spatial association with the temperature trends seen in the studied regions. On a broader scale, most of North America, eastern Asia, southern South America and New Zealand experience annual and summer wetting trends in precipitation (0-20 % century^{-1}, Figure A2) and surface (top 10 cm) soil moisture (0-1 kg m^{-2} century^{-1}, not shown). Next, we tested for a signal in the vegetation cover, as the dynamical vegetation model in UKESM1.2 allows for different plant functional types (PFTs) to compete for land

https://doi.org/10.5194/egusphere-2026-1733
Preprint. Discussion started: 8 May 2026

under changing climate conditions. As the various PFTs have different evapotranspiration rates, changes in vegetation cover can lead to significant differences in local water availability. As a result, we found a striking spatial symmetry between areas experiencing changes in the distribution of plant functional types (Figure 6) and cooling of TX5x (Figure 2). In particular, the four regions experiencing a strong cooling trend in swl-4.0 and swl-5.0 (Figure 3) all show an increase in the relative abundance of broadleaf evergreen (BdlEvg) vegetation over the same period. Throughout swl-4.0 and swl-5.0, BdlEvg vegetation expands poleward beyond the tropical and subtropical areas where it naturally occurs under historical conditions. Interestingly, the same trend does not apply to swl-3.0, in which very limited expansion of broadleaf and needleleaf evergreen vegetation occurs in the studied regions (Figure 7). Given that no substantial precipitation changes are registered in the studied regions across different stabilised scenarios (not shown), this suggests that the biome shifts produced by the model are mainly temperature dependent. In particular, it appears that some processes triggering the vegetation expansion occur at the boundary between a +3°C and +4°C global warming level (GWL, Figure 7a). Changes in mean temperatures, especially in the winter, are often responsible for biome shifts since they are a crucial factor in the establishment and survival of different tree species at mid-high latitudes (Xu et al., 2013; Kreyling, 2010). The role of mean temperature changes is further exemplified by the results from the negative emissions projection (swl-5.0-dn1.0, Figure 7b). Consistent with the stabilised runs, BdlEvg vegetation expansion in swl-5.0-dn1.0 stops when the GWL falls below +4°C with regression starting around +3.5°C GWL. An almost identical trend is observed in the other regions, with an initial expansion of broadleaf evergreen vegetation followed by a declining trend starting between +3.5°C and +4°C GWL (not shown). Figure 7c provides further evidence for the tight relationship between vegetation expansion and the evolution of regional TX5x. As previously shown (Figure 3), in swl-5.0 (purple) TX5x declines despite the increasing GWL. Similarly, the decrease in TX5x in swl-5.0-dn1.0 (blue) follows a different trajectory compared to the warming trend seen in the ramp-up. A comparison of the middle and right panels of Figure 7 suggests that this hysteresis is likely caused by the different vegetation cover found in the ramp-up and the negative emissions scenario. The initial BdlEvg vegetation expansion occurring in the negative emissions scenario accelerates the TX5x cooling relative to the GWL decline. As the BdlEvg vegetation cover shrinks over time, the cooling trend decelerates and TX5x eventually approaches the same values per GWL found in the ramp-up.

https://doi.org/10.5194/egusphere-2026-1733
Preprint. Discussion started: 8 May 2026

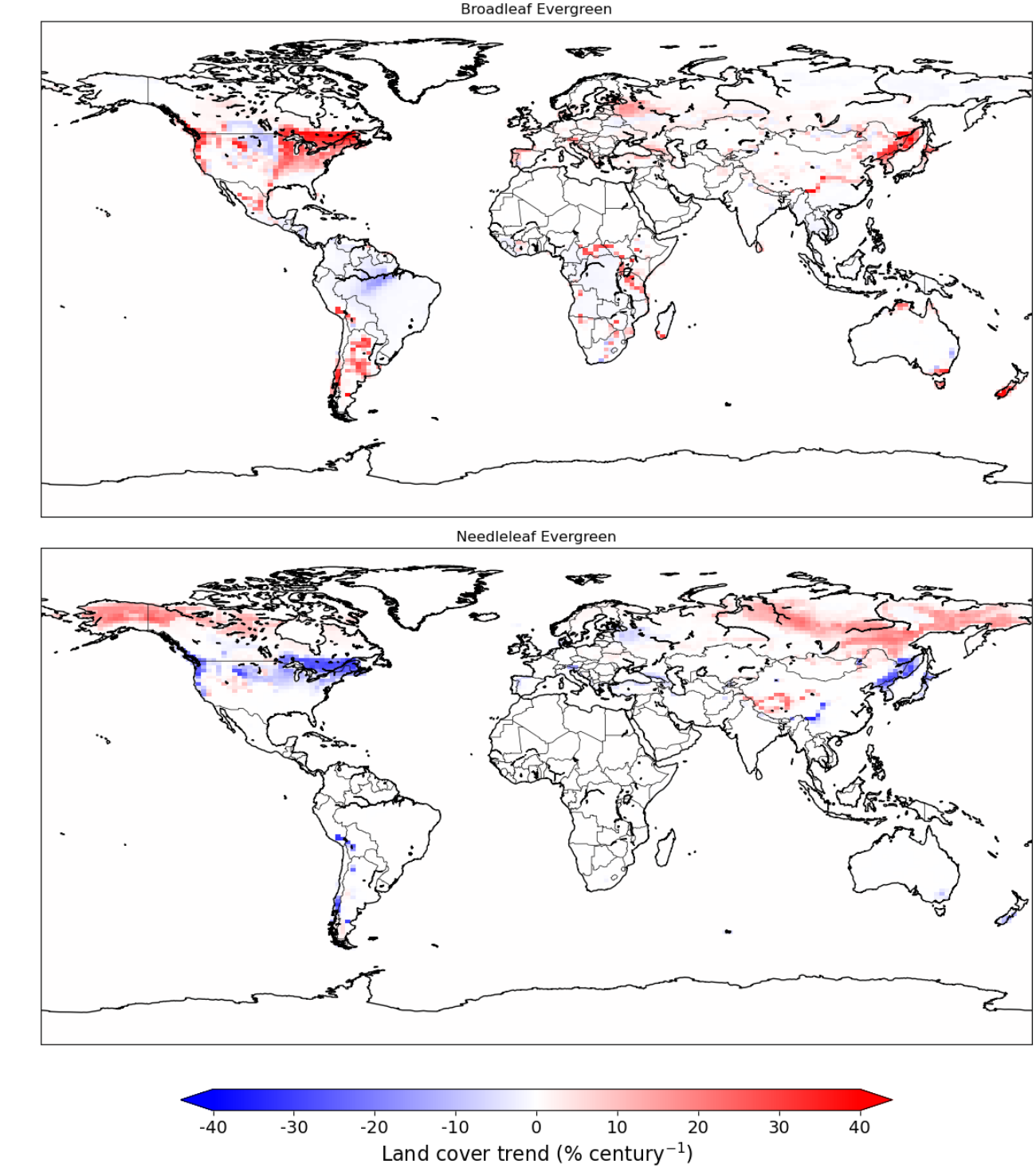

Figure 6. *Ensemble mean trend (% century^{-1}) in broadleaf evergreen (top) and needleleaf evergreen (bottom) vegetation land fraction in the first 250 years of swl-5.0.*

https://doi.org/10.5194/egusphere-2026-1733
Preprint. Discussion started: 8 May 2026

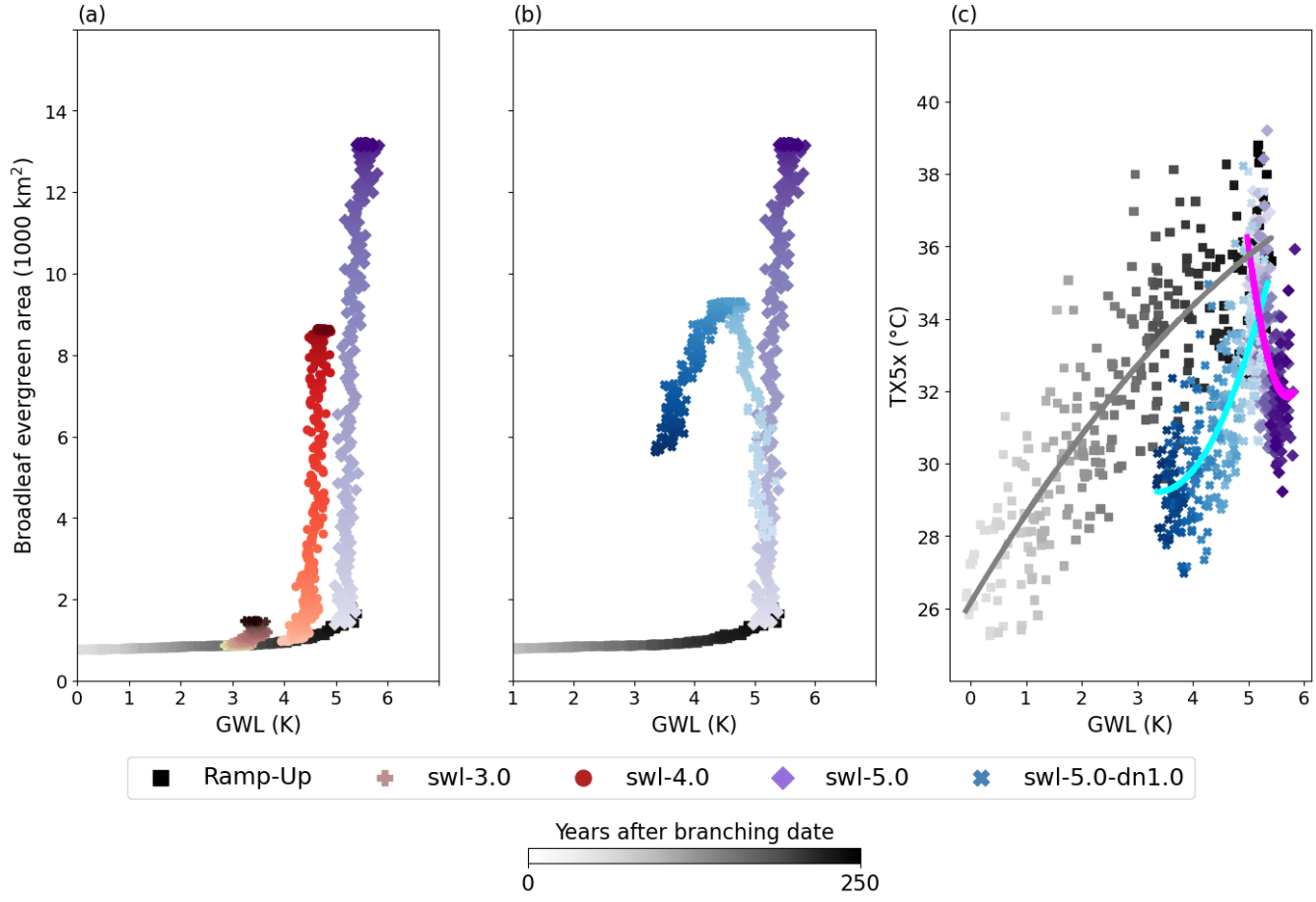

Figure 7. ***(a)*** *Evolution of broadleaf evergreen vegetation land area (1000 km^2) averaged across the studied North American region in the ramp-up (black), swl-3.0 (pink), swl-4.0 (red) and swl-5.0 (purple) runs against average global warming levels (GWL). GWLs are defined as the annual mean surface air temperature anomaly above the 31-year average around the ramp-up branching point from the piControl. Each dot represents the average one-year value, with all ensemble members of each run combined. The colour shading indicates the number of years after the branching point of each run.* ***(b)*** *Same as* ***(a)****, but comparing swl-5.0 with swl-5.0-dn1.0 (blue).* ***(c)*** *Evolution of TX5x (°C) in the ramp-up, swl-5.0 and swl-5.0-dn1.0 against GWL. The solid lines represent the second-order polynomial fit of TX5x against GWL in each run.*

Although some association with changes in mean temperature seems apparent, other factors must be playing a role in driving the biome shifts, as the affected regions are characterized by substantially different temperature regimes. This non-linearity is consistent with the design of the dynamic vegetation component of UKESM1.2 (Clark et al., 2011). While competition between plant functional types (PFTs) is ultimately influenced by temperature, several non-linear relationships control growth and expansion dynamics within and across PFTs based on changes in climate conditions, hence hindering the derivation of an absolute temperature threshold for change (Cox, 2001; Harper et al., 2016).

https://doi.org/10.5194/egusphere-2026-1733
Preprint. Discussion started: 8 May 2026

While the climatic drivers leading to the projected biome shifts are hard to disentangle, a variety of modelling and observational evidence supports their cooling effect on hot temperature extremes. A multi-model study by Alkama et al. (2022) shows that CMIP6 Earth System Models agree on the cooling effect produced by vegetation expansion on summer mean temperatures at mid-high latitudes in high-emission scenarios. The magnitude of the vegetation-induced cooling effect they find in the temperate and boreal regions (-0.2 to -0.4°C century^{-1}) is very similar to our results for a comparable level of global warming (Figure 2 swl-4.0 and swl-5.0), demonstrating that UKESM is not an outlier in the CMIP6 ensemble. Moreover, other studies confirmed that local changes in vegetation structure and abundance lead to regional and hemispheric impacts on climate conditions in Earth System Models due to the cascading effects of altered surface energy balance on atmospheric circulation (Swann et al., 2018; Devaraju et al., 2018; Lian et al., 2022). While seasonal and regional differences apply (Forzieri et al., 2017), the modelled cooling effect on summer temperatures is also supported by observational evidence from satellites showing how recent deforestation trends have produced a positive radiative forcing in the affected regions and vice-versa for afforestation (Duveiller et al., 2018; Li et al., 2023). Observational evidence also supports the cooling effects of broadleaf vegetation expansion seen in this study. Broadleaf plants have higher stomatal conductance than needleleaf (Baldocchi and Vogel, 1996), leading to higher transpiration and likely explaining the local increase in latent heat flux shown here (Figure 5). In the dynamic vegetation model this difference is mainly represented through the higher maximum rate of carboxylation and the higher critical humidity threshold parameters assigned to evergreen vegetation compared to deciduous (Harper et al., 2016). A further contribution to the cooling trend could originate from the higher albedo of broadleaf species (Houldcroft et al., 2009; Chen et al., 2018), which is captured by the model through a corresponding decrease in absorbed shortwave radiation at the regional scale (Figure A1).

The geography and the spatial extent of the projected biome shift might seem implausible under current climate conditions, but this transition is physically plausible in a +4°C and +5°C warmer world. Indeed, evergreen broadleaf vegetation has already been observed expanding in temperate climates under the influence of climate change (Walther et al., 2001). A study by Shin et al. (2022) found that the northern limit of broadleaf evergreen species distribution in South Korea has moved north by more than 1° latitude over the last decade, with species distribution modelling predicting an exponential expansion by the end of the century under high-emission conditions. Paleoclimatic evidence also shows how the latitudinal range of these plants can change dramatically with global warming, as it already occurred during the last deglaciation when they re-expanded into subtropical China (Zheng et al., 2023). Looking further back in time, fossil records from the Miocene (15 Ma), when global average temperatures were 3-4°C warmer than present, show how broadleaf evergreen vegetation extended well beyond 60°N and was the most abundant vegetation type across the mid-latitudes (Utescher et al., 2007; You et al., 2009). Alongside the expansion of broadleaf vegetation, a widespread increase in needleleaf evergreen vegetation occurs in subpolar North America, as well as eastern and central Siberia (Figure 6). These regions also see a noticeable cooling of TX5x in swl-5.0 despite warming in the mean (Figure 2), which is likely driven by the mitigation of the diurnal sensible heat flux in the summer months caused by the replacement of grasslands with high-canopy vegetation (Duveiller et al., 2018).

https://doi.org/10.5194/egusphere-2026-1733
Preprint. Discussion started: 8 May 2026

The body of evidence presented above suggests that the model representation of vegetation dynamics and the climate system response to changes in vegetation cover are plausible and self-consistent. Overall, the present results highlight the role of land cover changes as an important factor regulating the climate system response following CO_2 emissions cessation, as their relative impact increases once the anthropogenic forcing stops. Our findings suggest that including a far-sighted land use planning strategy in the current global warming mitigation and adaptation efforts could reap further benefits once climate stabilisation is achieved. Its potential in less idealised scenarios remains to be investigated but is supported from the literature (Searchinger et al., 2018; Fankhauser et al., 2022; King et al., 2024b). As further evidence, we find that the expansion of vegetation does not only affect the annual temperature extremes, but causes a more general reduction in the intraseasonal variance of summer (JJA) daily maximum temperatures (Figure 8). In the case of North American and Asian regions, the strongest decrease in the daily maximum temperature variance occurs for the swl-4.0 and swl-5.0 simulations (i.e., those with marked vegetation changes). Indeed, while emission cessation seems sufficient to halt the increase in variance found in the ramp-up run in all simulations, a marked reversal in trend magnitude only appears in swl-4.0 and swl-5.0. This difference appears even more clearly comparing the evolution of the summer temperature distribution between swl-3.0 and swl-5.0 in North America (Figure 8, right). Indeed, the negative shift in the mean and the shrinking of the hot temperature tail seen in swl-5.0 can be reconciled with the concomitant vegetation expansion, which is largely absent in swl-3.0 (Figure 7). To further support this relationship, Figure 8 shows how the same changes in JJA temperature variance seen in northeastern North America and Asia in swl-4.0 and swl-5.0 do not apply to central Europe [44-49°N ; 10-21°E], likely because Europe is not affected by any substantial vegetation shifts (Figure 6). Indeed, the expansion of BdlEvg vegetation cover is not sufficient to bring the daily maximum temperature mean and variance back to the piControl values, with swl-5.0 showing a greater difference from the unforced scenario compared to swl-3.0 even 200-250 years after emissions cessation. Yet, looking at swl-5.0, it is clear how the benefits of achieving zero emissions conditions for extreme temperature mitigation can be strongly affected by the changes in land cover. Thus, while our results indicate the possibility for large-scale afforestation to cause a reduction in the hot temperature extremes, opposite trends in land use changes could thwart the mean cooling effect brought by emissions cessation through a regional thermodynamic warming effect (Zhang et al., 2005; Butt et al., 2023).

https://doi.org/10.5194/egusphere-2026-1733
Preprint. Discussion started: 8 May 2026

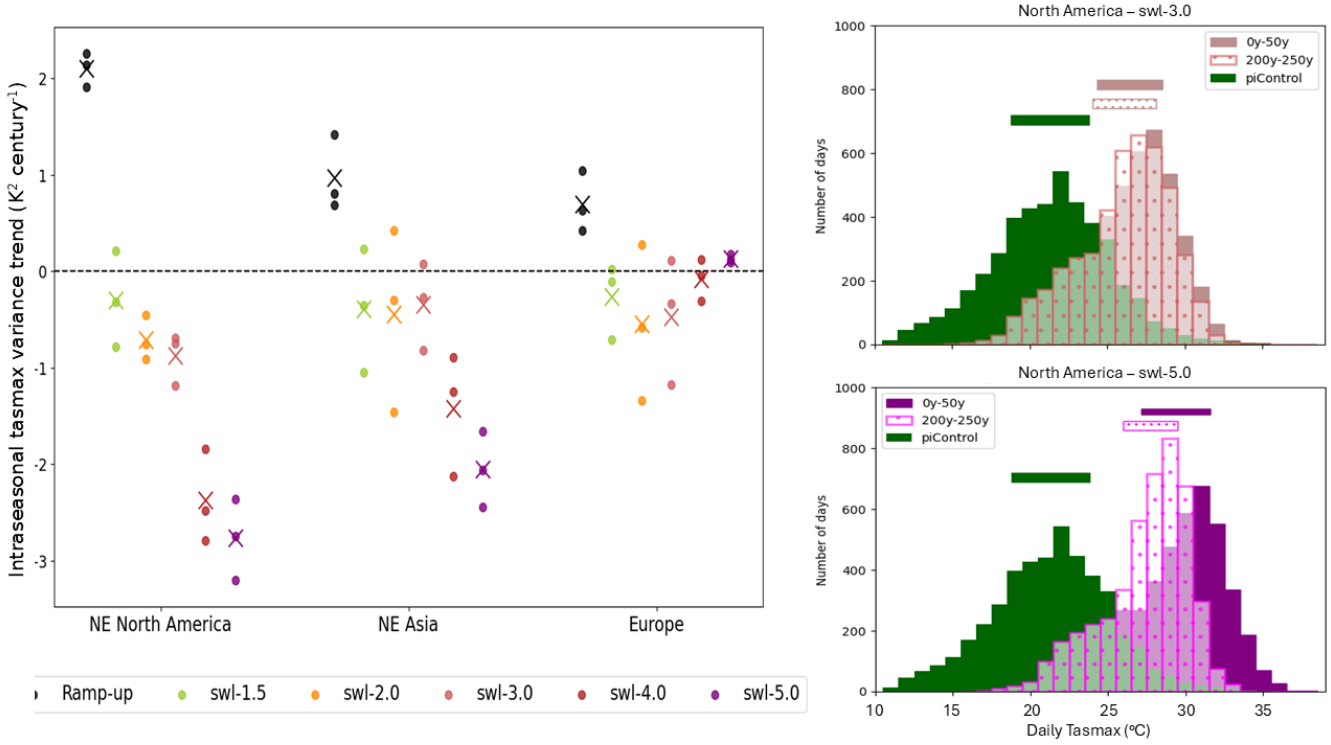

Figure 8. *Left: Intraseasonal variance trends for summer (JJA) daily maximum temperature (tasmax) in the studied regions in northeastern North America, northeastern Asia and Europe in the ramp-up and swl runs. For each scenario, the dots represent the individual ensemble members, while the cross identifies the ensemble mean. Right: Distribution of spatially averaged JJA daily maximum temperature in years 0-50 (coloured) and 200-250 (dotted) in the swl-3.0 (top) and swl-5.0 (bottom) runs in the studied northeastern North America region. The same distribution is shown in green for the last 50 years of the piControl run. The horizontal bars are a graphical representation of the interquartile range of each distribution.*

However, it is worth noting that the extent of the vegetation transitions observed in these projections would likely be strongly limited by a more realistic definition of land allocation dynamics. In these runs, vegetation is free to expand over most of the globe since cropland and urban areas are kept fixed at their pre-industrial level (Jones et al., 2025). Thus, while potentially achievable from a climatic perspective, the projected biome shifts would likely be confined to smaller pockets of land under future scenarios consistent with current and future land use and socio-economic trends. Consequently, the prominent cooling trends in annual hot temperature extremes at higher warming levels identified here may be a result of the highly idealised TIPMIP protocol. The extent to which they would occur in less idealised scenarios is unclear, but would likely be more limited. Evidence for this claim is found within these same projections and most likely explains why Europe, the only continent with considerable cropland area in the pre-industrial configuration that is used here, does not show a vegetation-induced TX5x cooling signal despite occupying the same latitudes as the other affected regions (Figures 2, 6, 8). Therefore, our results also serve as a reminder of the limits of highly idealised climate scenarios. While their fundamental value for exploring the response of the macro-processes governing the climate system under different forcing conditions is not questioned (Jones et al., 2025), there needs to be careful consideration of the implications of the approximations and assumptions embedded in them, especially

https://doi.org/10.5194/egusphere-2026-1733
Preprint. Discussion started: 8 May 2026

when finer-scale processes and feedbacks are considered. As the exploration of future climate conditions based on stabilised and net-negative emission scenarios is rapidly expanding, often based on novel and highly-idealised protocols (Jones et al., 2025, 2019; Keller et al., 2018; Sanderson et al., 2024), we need to ensure their unique experimental design is used to broaden our understanding of the climate system and that artificial results inapplicable to real-world conditions are identified where they occur (Baumberger et al., 2017). As shown here, this risk can be exacerbated by the plausibility and self-consistency of the results within the model and artifacts might be particularly hard to identify in the absence of a direct benchmark (such as land allocation in our case). Further results from other Earth System Models with dynamic vegetation schemes and using the same protocol will ultimately be needed to confirm whether our findings are model dependent or generally apply to the TIPMIP configuration. More broadly, a multi-model comparison will help contextualise our results and allow to constrain the large uncertainty still associated with the post zero emissions climate evolution (Randall et al., 2007).

4 Conclusions

The present study investigated temperature trends in the UKESM1.2 stabilised warming runs following the TIPMIP protocol (Jones et al., 2025). We find that global average air surface temperature keeps increasing after emissions stop in this model. Warming post emission cessation is significantly higher in +3°C to +5°C scenarios (0.23-0.24°C per century) compared to +1.5°C and +2°C (0.01-0.05°C per century). Strong regional gradients are found in mean temperature trends following emissions cessation, with most of the warming occurring in the SH as a result of the long-term heat release from the SO (Corner et al., 2023). The NH experiences a slight cooling of mean annual temperatures, which is more evident at the lower warming levels. This cooling pattern is regionally amplified for the annual temperature extremes (TXx and TX5x) in mid-latitude locations across the NH, and locally in the SH, in the swl-4.0 and swl-5.0 runs. Northeast North America experiences the greatest amount of cooling for TX5x, exceeding -1.5°C per century in swl-5.0.

The regional analysis of the dynamic and thermodynamic drivers of heat extremes revealed that the cooling pattern is primarily explained by an increased partitioning of the total surface net radiation into latent rather than sensible heat flux. This change in the partitioning of the surface heat fluxes is associated with the poleward expansion of broadleaf and needleleaf evergreen vegetation at the expenses of deciduous trees and grasslands. The expansion of tree vegetation reduces the summer daily maximum temperature variance in the studied regions, shrinking the warm tail of the temperature distribution. As shown in previous modelling and observational studies, large-scale biome shifts can be responsible for regional cooling of heat extremes due to the increased transpiration rates and summer surface albedo.

While plausible and self-consistent within the model, these results are greatly influenced by the experimental protocol, in which anthropogenic land use is kept fixed at the pre-industrial level. Thus, the extent and the magnitude of the projected biome shifts, and the associated cooling effect, would likely be substantially limited in real-world conditions, even under minimal land-disturbance scenarios. This highlights the potential limitations of highly-idealised scenarios, showing how such

https://doi.org/10.5194/egusphere-2026-1733
Preprint. Discussion started: 8 May 2026

assumptions can generate possibly unrealistic responses in climate models.

Nevertheless, our results show the important role that land use changes can play in mitigating heat-related hazards, with its relative impact increasing after emission cessation. Without this contribution, mean and extreme temperatures would not decline as significantly under zero emissions conditions, especially in the SH. Thus, our study aligns with a growing body of evidence suggesting that the effects of global warming stabilisation on climate extremes can have sharp regional variations (Dittus et al., 2024; Cassidy et al., 2024; Alastrué de Asenjo et al., 2025) and identifies land-atmosphere feedbacks as one of the mechanisms explaining them.

https://doi.org/10.5194/egusphere-2026-1733
Preprint. Discussion started: 8 May 2026

Code and data availability. Selected CMORised output from the UKESM TIPMIP ensemble can be publicly accessed at https://gws-access.jasmin.ac.uk/public/ukesm/TerraFIRMA. The full simulation output are archived at the UK Met Office and are available for research purposes through the JASMIN platform (www.jasmin.ac.uk) maintained by the Centre for Environmental Data Analysis (CEDA); for details please contact UM_collaboration@metoffice.gov.uk, referencing this paper. The code used for the analysis will be made publicly available upon acceptance of the manuscript.

https://doi.org/10.5194/egusphere-2026-1733
Preprint. Discussion started: 8 May 2026

Appendix A

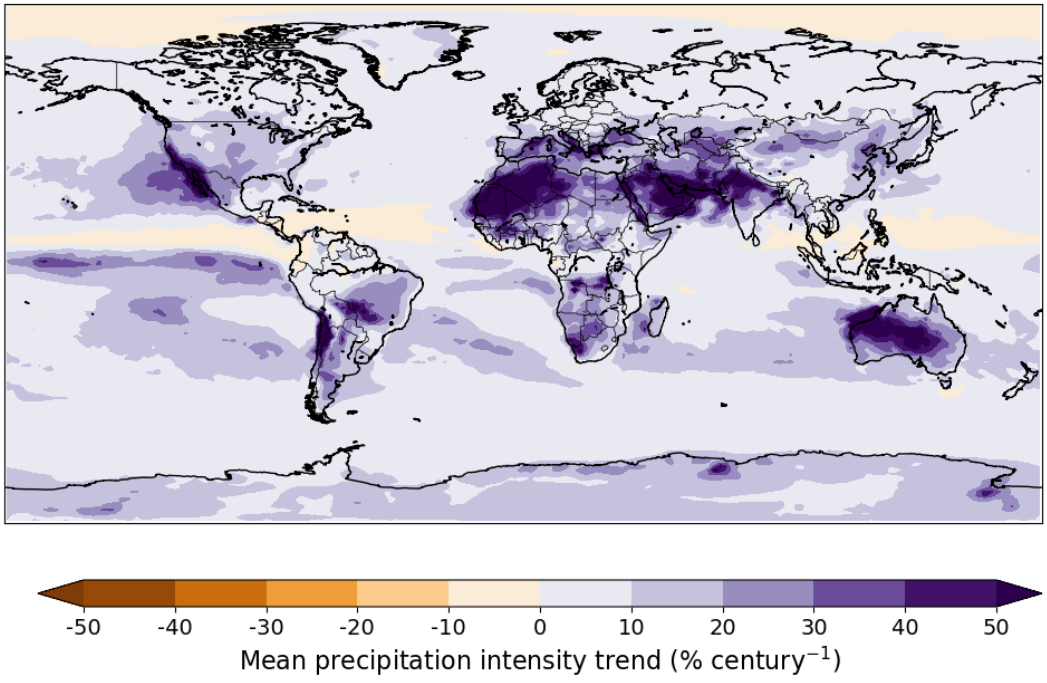

Figure A1. *Ensemble mean trend in annual mean precipitation intensity (%/century) in the first 250 years of swl-5.0.*

https://doi.org/10.5194/egusphere-2026-1733
Preprint. Discussion started: 8 May 2026

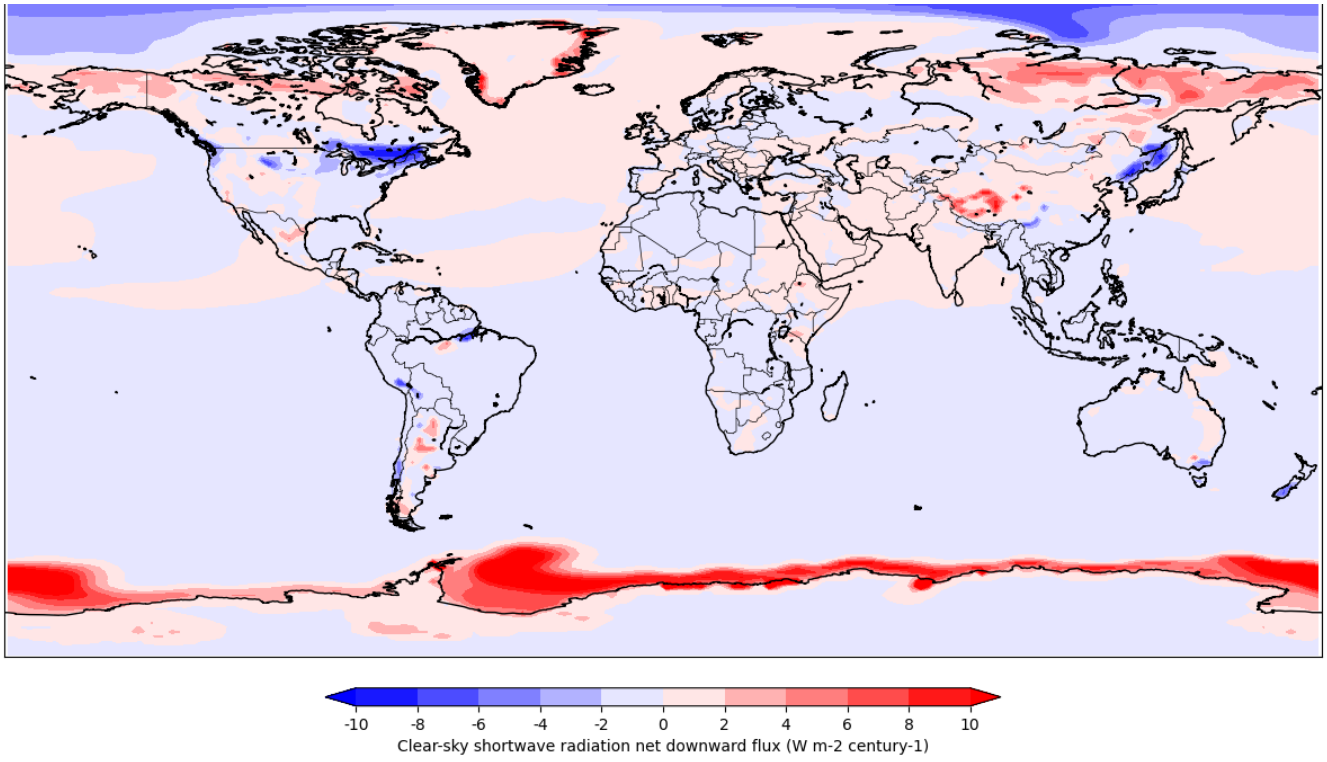

Figure A2. *Ensemble mean trend in annual mean clear-sky net downward summer shortwave radiation flux (W* m^{-2} *century* $^{-1}$*) in the first 250 years of swl-5.0. The net flux is calculated subtracting the upward shortwave radiation flux from the total downward shortwave radiation flux.*

https://doi.org/10.5194/egusphere-2026-1733
Preprint. Discussion started: 8 May 2026

Author contributions. Conceptualization: AR, AD, EH, RS; Data curation: AR; Formal analysis: AR; Funding acquisition: AD; Methodology: AR, AD, EH, RS; Supervision: AD, EH, RS, EF; Writing (original draft): AR; Writing (review and editing): AD, EH, RS, EF.

Competing interests. The authors declare that they have no conflict of interest.

Acknowledgements. AR was funded by the NERC SCENARIO Doctoral Training Partnership NE/S007261/1. AD was funded by NERC Independent Research Fellowship NE/X017850/1.

This research has been supported by TerraFIRMA "Future Impacts, Risks and Mitigation Actions in a changing Earth system" is funded by the UKRI Natural Environment Research Council (grant reference NE/W004895/1); European Union Horizon 2020 project ESM2025 (grant agreement no. 101003536); Horizon Europe project OptimESM "Optimal High Resolution Earth System Models for Exploring Future Climate Changes" (grant agreement no. 101081193); the UK government's Horizon Europe funding guarantee (grant numbers, 10103098, 10043072); TipESM "Exploring Tipping Points and Their Impacts Using Earth System Models" funded by the European Union (grant agreement no. 101137673. DOI: 10.3030/101137673, TipESM contribution no. XX).

The authors acknowledge Colin Jones, Jeremy Walton, Robin Smith, Spencer Liddicoat and Eddy Robertson for their help and support.

https://doi.org/10.5194/egusphere-2026-1733
Preprint. Discussion started: 8 May 2026

References

Alastrué de Asenjo, E., King, A. D., and Ziehn, T.: European heat extremes under net-zero emissions, Environmental Research Letters, 20, 074 029, https://doi.org/10.1088/1748-9326/addee4, 2025.

Alkama, R., Forzieri, G., Duveiller, G., Grassi, G., Liang, S., and Cescatti, A.: Vegetation-based climate mitigation in a warmer and greener World, Nature Communications, 13, https://doi.org/10.1038/s41467-022-28305-9, 2022.

Baldocchi, D. D. and Vogel, C. A.: Energy and CO2 flux densities above and below a temperate broad-leaved forest and a boreal pine forest, Tree Physiology, 16, 5–16, https://doi.org/10.1093/treephys/16.1-2.5, 1996.

Barriopedro, D., García-Herrera, R., Ordóñez, C., Miralles, D. G., and Salcedo-Sanz, S.: Heat Waves: Physical Understanding and Scientific Challenges, Reviews of Geophysics, 61, https://doi.org/10.1029/2022RG000780, 2023.

Baumberger, C., Knutti, R., and Hadorn, G. H.: Building confidence in climate model projections: an analysis of inferences from fit, Wiley Interdisciplinary Reviews: Climate Change, 8, https://doi.org/10.1002/wcc.454, 2017.

Butt, E. W., Baker, J. C., Bezerra, F. G. S., von Randow, C., Aguiar, A. P., and Spracklen, D. V.: Amazon deforestation causes strong regional warming, Proceedings of the National Academy of Sciences of the United States of America, 120, https://doi.org/10.1073/pnas.2309123120, 2023.

Cassidy, L. J., King, A. D., Brown, J. R., MacDougall, A. H., Ziehn, T., Min, S. K., and Jones, C. D.: Regional temperature extremes and vulnerability under net zero CO2 emissions, Environmental Research Letters, 19, https://doi.org/10.1088/1748-9326/ad114a, 2024.

Chen, D., Loboda, T. V., He, T., Zhang, Y., and Liang, S.: Strong cooling induced by stand-replacing fires through albedo in Siberian larch forests, Scientific Reports, 8, 4821, https://doi.org/10.1038/s41598-018-23253-1, 2018.

Clark, D. B., Mercado, L. M., Sitch, S., Jones, C. D., Gedney, N., Best, M. J., Pryor, M., Rooney, G. G., Essery, R. L. H., Blyth, E., Boucher, O., Harding, R. J., Huntingford, C., and Cox, P. M.: The Joint UK Land Environment Simulator (JULES), model description – Part 2: Carbon fluxes and vegetation dynamics, Geoscientific Model Development, 4, 701–722, https://doi.org/10.5194/gmd-4-701-2011, 2011.

Corner, S. P., Siegert, M., Ceppi, P., Fox-Kemper, B., Frölicher, T. L., Gallego-Sala, A., Haigh, J., Hegerl, G. C., Jones, C. D., Knutti, R., Koven, C. D., MacDougall, A. H., Meinshausen, M., Nicholls, Z., Sallée, J. B., Sanderson, B. M., Séférian, R., Turetsky, M., Williams, R. G., Zaehle, S., and Rogelj, J.: The Zero Emissions Commitment and climate stabilization, Frontiers in Science, 1, https://doi.org/10.3389/fsci.2023.1170744, 2023.

Costa, D. F., Gomes, H. B., Silva, M. C. L., and Zhou, L.: The most extreme heat waves in Amazonia happened under extreme dryness, Climate Dynamics, 59, https://doi.org/10.1007/s00382-021-06134-8, 2022.

Cox, P. M.: Description of the TRIFFID Dynamic Global Vegetation Model, Hadley Centre technical note, 24, 2001.

Deser, C. and Phillips, A. S.: Forced and Internal Components of Winter Air Temperature Trends over North America during the past 50 Years: Mechanisms and Implications*, Journal of Climate, 29, 2237–2258, https://doi.org/10.1175/JCLI-D-15-0304.s1, 2016.

Devaraju, N., Noblet-Ducoudré, N. D., Quesada, B., and Bala, G.: Quantifying the Relative Importance of Direct and Indirect Biophysical Effects of Deforestation on Surface Temperature and Teleconnections, Journal of Climate, 31, 3811–3829, https://doi.org/10.1175/JCLI-D-17-0563.s1, 2018.

Dittus, A. J., Collins, M., Sutton, R., and Hawkins, E.: Reversal of Projected European Summer Precipitation Decline in a Stabilizing Climate, Geophysical Research Letters, 51, https://doi.org/10.1029/2023GL107448, 2024.

Donat, M. G., Pitman, A. J., and Seneviratne, S. I.: Regional warming of hot extremes accelerated by surface energy fluxes, Geophysical Research Letters, 44, 7011–7019, https://doi.org/10.1002/2017GL073733, 2017.

https://doi.org/10.5194/egusphere-2026-1733
Preprint. Discussion started: 8 May 2026

Duveiller, G., Hooker, J., and Cescatti, A.: The mark of vegetation change on Earth's surface energy balance, Nature Communications, 9, https://doi.org/10.1038/s41467-017-02810-8, 2018.

Fankhauser, S., Smith, S. M., Allen, M., Axelsson, K., Hale, T., Hepburn, C., Kendall, J. M., Khosla, R., Lezaun, J., Mitchell-Larson, E., Obersteiner, M., Rajamani, L., Rickaby, R., Seddon, N., and Wetzer, T.: The meaning of net zero and how to get it right, https://doi.org/10.1038/s41558-021-01245-w, 2022.

Fischer, E. M., Seneviratne, S. I., Lüthi, D., and Schär, C.: Contribution of land-atmosphere coupling to recent European summer heat waves, Geophysical Research Letters, 34, https://doi.org/https://doi.org/10.1029/2006GL029068, 2007.

Forzieri, G., Alkama, R., Miralles, D. G., and Cescatti, A.: Satellites reveal contrasting responses of regional climate to the widespread greening of Earth, Science, 356, https://doi.org/10.1126/science.aal1727, 2017.

Frölicher, T. L., Winton, M., and Sarmiento, J. L.: Continued global warming after CO2 emissions stoppage, Nature Climate Change, 4, 40–44, https://doi.org/10.1038/nclimate2060, 2014.

Gibbs, L., Jones, C. D., Jones, C., Andrews, T., Liddicoat, S., Wiltshire, A. J., Robertson, E., Williams, R. G., de Mora, L., Walton, J., Dittus, A., Swaminathan, R., Ceppi, P., Smith, R. S., and Rumbold, S. T.: Zero Emissions Commitment depends on warming level., available as pre-print https://doi.org/10.21203/rs.3.rs-8346352/v1.

Gillett, N. P., Arora, V. K., Zickfeld, K., Marshall, S. J., and Merryfield, W. J.: Ongoing climate change following a complete cessation of carbon dioxide emissions, Nature Geoscience, 4, 83–87, https://doi.org/10.1038/ngeo1047, 2011.

Harper, A. B., Cox, P. M., Friedlingstein, P., Wiltshire, A. J., Jones, C. D., Sitch, S., Mercado, L. M., Groenendijk, M., Robertson, E., Kattge, J., Bönisch, G., Atkin, O. K., Bahn, M., Cornelissen, J., Ülo Niinemets, Onipchenko, V., Peñuelas, J., Poorter, L., Reich, P. B., Soudzilovskaia, N. A., and Bodegom, P. V.: Improved representation of plant functional types and physiology in the Joint UK Land Environment Simulator (JULES v4.2) using plant trait information, Geoscientific Model Development, 9, 2415–2440, https://doi.org/10.5194/gmd-9-2415-2016, 2016.

Harper, A. B., Wiltshire, A. J., Cox, P. M., Friedlingstein, P., Jones, C. D., Mercado, L. M., Sitch, S., Williams, K., and Duran-Rojas, C.: Vegetation distribution and terrestrial carbon cycle in a carbon cycle configuration of JULES4.6 with new plant functional types, Geoscientific Model Development, 11, https://doi.org/10.5194/gmd-11-2857-2018, 2018.

Hoegh-Guldberg, O., Bindi, M., Brown, S., Camilloni, I., Diedhiou, A., Djalante, R., Ebi, K. L., Engelbrecht, F., Guangsheng, Z., Guiot, J., Hijioka, Y., Mehrotra, S., Payne, A., Seneviratne, S. I., Thomas, A., and Warren, R.: Impacts of 1.5°C of Global Warming on Natural and Human Systems, in: Global Warming of 1.5°C: An IPCC Special Report on the impacts of global warming of 1.5°C above pre-industrial levels and related global greenhouse gas emission pathways, in the context of strengthening the global response to the threat of climate change, sustainable development, and efforts to eradicate poverty, edited by Masson-Delmotte, V., Zhai, P., Pörtner, H.-O., Roberts, D., Skea, J., Shukla, P. R., Pirani, A., Moufouma-Okia, W., Péan, C., Pidcock, R., Connors, S., Matthews, J. B. R., Chen, Y., Zhou, X., Gomis, M. I., Lonnoy, E., Maycock, T., Tignor, M., and Waterfield, T., World Meteorological Organization, Geneva, Switzerland, ISBN 978-92-9169-151-7, https://www.ipcc.ch/sr15/, 2018.

Horowitz, R. L., McKinnon, K. A., and Simpson, I. R.: Circulation and Soil Moisture Contributions to Heatwaves in the United States, Journal of Climate, 35, 8031–8048, https://doi.org/https://doi.org/10.1175/JCLI-D-21-0156.1, 2022.

Houldcroft, C. J., Grey, W. M., Barnsley, M., Taylor, C. M., Los, S. O., and North, P. R.: New vegetation Albedo parameters and global fields of soil background Albedo derived from MODIS for use in a climate model, Journal of Hydrometeorology, 10, https://doi.org/10.1175/2008JHM1021.1, 2009.

https://doi.org/10.5194/egusphere-2026-1733
Preprint. Discussion started: 8 May 2026

Jones, C., Bossert, I., Dennis, D. P., Jeffery, H., Jones, C. D., Koenigk, T., Loriani, S., Sanderson, B., Séférian, R., Wyser, K., Yang, S., Abe, M., Bathiany, S., Braconnot, P., Brovkin, V., Burger, F. A., Cadule, P., Castruccio, F. S., Danabasoglu, G., Dittus, A., Donges, J. F., Fröb, F., Frölicher, T., Georgievski, G., Guo, C., Hu, A., Lawrence, P., Lerner, P., Licón-Saláiz, J., Otto-Bliesner, B., Romanou, A., Shevliakova, E., Silvy, Y., Swingedouw, D., Tjiputra, J., Walton, J., Wiltshire, A., Winkelmann, R., Wood, R., Yokohata, T., and Ziehn, T.: The TIPMIP Earth system model experiment protocol: phase 1, Geoscientific Model Development, https://doi.org/10.5194/egusphere-2025-3604, 2025.

Jones, C. D., Frölicher, T. L., Koven, C., MacDougall, A. H., Matthews, H. D., Zickfeld, K., Rogelj, J., Tokarska, K. B., Gillett, N. P., Ilyina, T., Meinshausen, M., Mengis, N., Séférian, R., Eby, M., and Burger, F. A.: The Zero Emissions Commitment Model Intercomparison Project (ZECMIP) contribution to C4MIP: Quantifying committed climate changes following zero carbon emissions, Geoscientific Model Development, 12, https://doi.org/10.5194/gmd-12-4375-2019, 2019.

Keller, D. P., Lenton, A., Scott, V., Vaughan, N. E., Bauer, N., Ji, D., Jones, C. D., Kravitz, B., Muri, H., and Zickfeld, K.: The Carbon Dioxide Removal Model Intercomparison Project (CDRMIP): Rationale and experimental protocol for CMIP6, Geoscientific Model Development, 11, https://doi.org/10.5194/gmd-11-1133-2018, 2018.

King, A. D., Ziehn, T., Chamberlain, M., Borowiak, A. R., Brown, J. R., Cassidy, L., Dittus, A. J., Grose, M., Maher, N., Paik, S., Perkins-Kirkpatrick, S. E., and Sengupta, A.: Exploring climate stabilisation at different global warming levels in ACCESS-ESM-1.5, Earth System Dynamics, 15, 1353–1383, https://doi.org/10.5194/esd-15-1353-2024, 2024a.

King, J. A., Weber, J., Lawrence, P., Roe, S., Swann, A. L., and Martin, M. V.: Global and regional hydrological impacts of global forest expansion, Biogeosciences, 21, https://doi.org/10.5194/bg-21-3883-2024, 2024b.

Kreyling, J.: Winter climate change: A critical factor for temperate vegetation performance, Ecology, 91, https://doi.org/10.1890/09-1160.1, 2010.

Lee, J.-Y., Marotzke, J., Bala, G., Cao, L., Corti, S., Dunne, J., Engelbrecht, F., Fischer, E., Fyfe, J., Jones, C., Maycock, A., Mutemi, J., Ndiaye, O., Panickal, S., and Zhou, T.: Future Global Climate: Scenario-Based Projections and Near-Term Information, in: Climate Change 2021: The Physical Science Basis. Contribution of Working Group I to the Sixth Assessment Report of the Intergovernmental Panel on Climate Change, edited by Masson-Delmotte, V., Zhai, P., Pirani, A., Connors, S. L., Péan, C., Berger, S., Caud, N., Chen, Y., Goldfarb, L., Gomis, M. I., Huang, M., Leitzell, K., Lonnoy, E., Matthews, J. B. R., Maycock, T. K., Waterfield, T., Yelekçi, O., Yu, R., and Zhou, B., book section 4, pp. 553–672, Cambridge University Press, Cambridge, UK and New York, NY, USA, https://doi.org/10.1017/9781009157896.006, 2021.

Li, Y., Li, Z. L., Wu, H., Zhou, C., Liu, X., Leng, P., Yang, P., Wu, W., Tang, R., Shang, G. F., and Ma, L.: Biophysical impacts of earth greening can substantially mitigate regional land surface temperature warming, Nature Communications, 14, https://doi.org/10.1038/s41467-023-35799-4, 2023.

Lian, X., Jeong, S., Park, C. E., Xu, H., Li, L. Z., Wang, T., Gentine, P., Peñuelas, J., and Piao, S.: Biophysical impacts of northern vegetation changes on seasonal warming patterns, Nature Communications, 13, https://doi.org/10.1038/s41467-022-31671-z, agrees that vegetation greenning has cooling effect, especially visible in summer temperatures.

Go to section "Driving processes of the seasonal vegetation-climate feedback". Tries to understand which are the contributions of vegetation changes to temperature., 2022.

MacDougall, A. H., Frölicher, T. L., Jones, C. D., Rogelj, J., DamonMatthews, H., Zickfeld, K., Arora, V. K., Barrett, N. J., Brovkin, V., Burger, F. A., Eby, M., Eliseev, A. V., Hajima, T., Holden, P. B., Jeltsch-Thömmes, A., Koven, C., Mengis, N., Menviel, L., Michou, M., Mokhov, I. I., Oka, A., Schwinger, J., Séférian, R., Shaffer, G., Sokolov, A., Tachiiri, K., Tjiputra, J., Wiltshire, A., and Ziehn, T.: Is there warming in the pipeline? A multi-model analysis of the Zero Emissions Commitment from CO2, Biogeosciences, 17, 2987–3016, https://doi.org/10.5194/bg-17-2987-2020, 2020.

https://doi.org/10.5194/egusphere-2026-1733
Preprint. Discussion started: 8 May 2026

Merrifield, A., Lehner, F., Xie, S. P., and Deser, C.: Removing Circulation Effects to Assess Central U.S. Land-Atmosphere Interactions in the CESM Large Ensemble, Geophysical Research Letters, 44, 9938–9946, https://doi.org/10.1002/2017GL074831, 2017.

Miralles, D. G., Gentine, P., Seneviratne, S. I., and Teuling, A. J.: Land–atmospheric feedbacks during droughts and heatwaves: state of the science and current challenges, Annals of the New York Academy of Sciences, 1436, 19–35, https://doi.org/10.1111/nyas.13912, 2019.

Mulcahy, J. P., Jones, C. G., Rumbold, S. T., Kuhlbrodt, T., Dittus, A. J., Blockley, E. W., Yool, A., Walton, J., Hardacre, C., Andrews, T., Bodas-Salcedo, A., Stringer, M., Mora, L. D., Harris, P., Hill, R., Kelley, D., Robertson, E., and Tang, Y.: UKESM1.1: development and evaluation of an updated configuration of the UK Earth System Model, Geoscientific Model Development, 16, https://doi.org/10.5194/gmd-16-1569-2023, 2023.

Perkins, S. E., Argüeso, D., and White, C. J.: Relationships between climate variability, soil moisture, and Australian heatwaves, Journal of Geophysical Research, 120, 8144–8164, https://doi.org/10.1002/2015JD023592, 2015.

Perkins-Kirkpatrick, S., Palmer, L., King, A., and Ziehn, T.: Heatwaves in a net zero World, Environmental Research: Climate, 4, https://doi.org/10.1088/2752-5295/ae0ea4, 2025.

Quesada, B., Vautard, R., Yiou, P., Hirschi, M., and Seneviratne, S. I.: Asymmetric European summer heat predictability from wet and dry southern winters and springs, Nature Climate Change, 2, 736–741, https://doi.org/10.1038/nclimate1536, 2012.

Randall, D. A., Wood, R. A., Bony, S., Colman, R., Fichefet, T., Fyfe, J., Kattsov, V., Pitman, A., Shukla, J., Srinivasan, J., et al.: Climate models and their evaluation, in: Climate change 2007: The physical science basis. Contribution of Working Group I to the Fourth Assessment Report of the IPCC (FAR), pp. 589–662, Cambridge University Press, 2007.

Russo, S., Sillmann, J., Sippel, S., Barcikowska, M. J., Ghisetti, C., Smid, M., and O'Neill, B.: Half a degree and rapid socioeconomic development matter for heatwave risk, Nature Communications, 10, 136, https://doi.org/10.1038/s41467-018-08070-4, 2019.

Sanderson, B. M., Booth, B. B. B., Dunne, J., Eyring, V., Fisher, R. A., Friedlingstein, P., Gidden, M. J., Hajima, T., Jones, C. D., Jones, C. G., King, A., Koven, C. D., Lawrence, D. M., Lowe, J., Mengis, N., Peters, G. P., Rogelj, J., Smith, C., Snyder, A. C., Simpson, I. R., Swann, A. L. S., Tebaldi, C., Ilyina, T., Schleussner, C.-F., Séférian, R., Samset, B. H., van Vuuren, D., and Zaehle, S.: The need for carbon-emissions-driven climate projections in CMIP7, Geoscientific Model Development, 17, 8141–8172, https://doi.org/10.5194/gmd-17-8141-2024, 2024.

Searchinger, T. D., Wirsenius, S., Beringer, T., and Dumas, P.: Assessing the efficiency of changes in land use for mitigating climate change, Nature, 564, https://doi.org/10.1038/s41586-018-0757-z, 2018.

Seneviratne, S. I., Corti, T., Davin, E. L., Hirschi, M., Jaeger, E. B., Lehner, I., Orlowsky, B., and Teuling, A. J.: Investigating soil moisture-climate interactions in a changing climate: A review, https://doi.org/10.1016/j.earscirev.2010.02.004, 2010.

Shin, S., Kim, J. H., Kang, D., Kim, J. S., Kang, H. G., Jang, H. D., Lee, J., Han, J. E., and Oh, H. K.: Northern distribution limits and future suitable habitats of warm temperate evergreen broad-leaved tree species designated as climate-sensitive biological indicator species in South Korea, Journal of Ecology and Environment, 46, https://doi.org/10.5141/jee.22.053, 2022.

Siahaan, A., Smith, R. S., Holland, P. R., Jenkins, A., Gregory, J. M., Lee, V., Mathiot, P., Payne, A. J., Ridley, J. K., and Jones, C. G.: The Antarctic contribution to 21st-century sea-level rise predicted by the UK Earth System Model with an interactive ice sheet, Cryosphere, 16, https://doi.org/10.5194/tc-16-4053-2022, 2022.

Smith, R. S., Mathiot, P., Siahaan, A., Lee, V., Cornford, S. L., Gregory, J. M., Payne, A. J., Jenkins, A., Holland, P. R., Ridley, J. K., and Jones, C. G.: Coupling the U.K. Earth System Model to Dynamic Models of the Greenland and Antarctic Ice Sheets, Journal of Advances in Modeling Earth Systems, 13, https://doi.org/10.1029/2021MS002520, 2021.

https://doi.org/10.5194/egusphere-2026-1733
Preprint. Discussion started: 8 May 2026

Swann, A. L., Laguë, M. M., Garcia, E. S., Field, J. P., Breshears, D. D., Moore, D. J., Saleska, S. R., Stark, S. C., Villegas, J. C., Law, D. J., and Minor, D. M.: Continental-scale consequences of tree die-offs in North America: Identifying where forest loss matters most, Environmental Research Letters, 13, https://doi.org/10.1088/1748-9326/aaba0f, 2018.

Ukkola, A. M., Pitman, A. J., Donat, M. G., Kauwe, M. G. D., and Angélil, O.: Evaluating the Contribution of Land-Atmosphere Coupling to Heat Extremes in CMIP5 Models, Geophysical Research Letters, 45, https://doi.org/10.1029/2018GL079102, 2018.

Utescher, T., Erdei, B., François, L., and Mosbrugger, V.: Tree diversity in the Miocene forests of Western Eurasia, Palaeogeography, Palaeoclimatology, Palaeoecology, 253, 226–250, https://doi.org/https://doi.org/10.1016/j.palaeo.2007.03.041, 2007.

Walther, G.-R., Carraro, G., and Klötzli, F.: Evergreen broad-leaved species as indicators for climate change, pp. 151–162, Springer, 2001.

Winkelmann, R., Dennis, D. P., Donges, J. F., Loriani, S., Klose, A. K., Abrams, J. F., Alvarez-Solas, J., Albrecht, T., Armstrong McKay, D., Bathiany, S., Blasco Navarro, J., Brovkin, V., Burke, E., Danabasoglu, G., Donner, R. V., Drüke, M., Georgievski, G., Goelzer, H., Harper, A. B., Hegerl, G., Hirota, M., Hu, A., Jackson, L. C., Jones, C., Kim, H., Koenigk, T., Lawrence, P., Lenton, T. M., Liddy, H., Licón-Saláiz, J., Menthon, M., Montoya, M., Nitzbon, J., Nowicki, S., Otto-Bliesner, B., Pausata, F., Rahmstorf, S., Ramin, K., Robinson, A., Rockström, J., Romanou, A., Sakschewski, B., Schädel, C., Sherwood, S., Smith, R. S., Steinert, N. J., Swingedouw, D., Willeit, M., Weijer, W., Wood, R., Wyser, K., and Yang, S.: The Tipping Points Modelling Intercomparison Project (TIPMIP): Assessing tipping point risks in the Earth system, EGUsphere, 2025, 1–52, https://doi.org/10.5194/egusphere-2025-1899, 2025.

WMO: WMO confirms 2024 as warmest year on record at about 1.55°C above pre-industrial level, https://wmo.int/news/media-centre/wmo-confirms-2024-warmest-year-record-about-155degc-above-pre-industrial-level, 2025.

Xu, L., Myneni, R. B., Chapin, F. S., Callaghan, T. V., Pinzon, J. E., Tucker, C. J., Zhu, Z., Bi, J., Ciais, P., Tømmervik, H., Euskirchen, E. S., Forbes, B. C., Piao, S. L., Anderson, B. T., Ganguly, S., Nemani, R. R., Goetz, S. J., Beck, P. S., Bunn, A. G., Cao, C., and Stroeve, J. C.: Temperature and vegetation seasonality diminishment over northern lands, Nature Climate Change, 3, https://doi.org/10.1038/nclimate1836, 2013.

You, Y., Huber, M., Müller, R. D., Poulsen, C. J., and Ribbe, J.: Simulation of the Middle Miocene Climate Optimum, Geophysical Research Letters, 36, https://doi.org/https://doi.org/10.1029/2008GL036571, 2009.

Zhang, J., Dong, W., Wu, L., Wei, J., Chen, P., and Lee, D. K.: Impact of land use changes on surface warming in China, Advances in Atmospheric Sciences, 22, https://doi.org/10.1007/bf02918748, 2005.

Zheng, Z., Chen, C., Huang, K., Zhang, X., Kershaw, P., Cheng, J., Li, J., Yue, Y., Wan, Q., Zhang, Y., Tang, Y., Wang, M., Xiao, X., and Cheddadi, R.: Holocene warming and evergreen/deciduous forest replacement across eastern China, Quaternary Science Reviews, 307, 108 057, https://doi.org/https://doi.org/10.1016/j.quascirev.2023.108057, 2023.